ISSN 1387-2176, Volume 12, Number 5

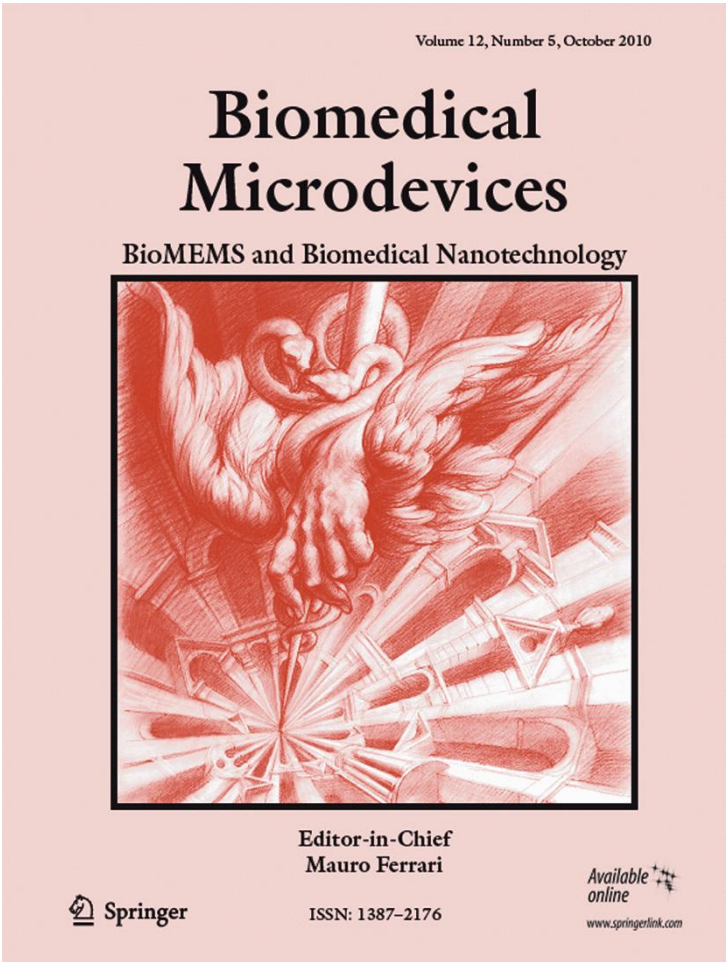

Biomed Microdevices (2010) 12:849–854
DOI 10.1007/s10544-010-9439-9

Fluidic measurement of electric field sensitivity of Ti-GaAs Schottky junction gated field effect biosensors

Woo-Jin Chang · Ho-Jun Suk · A. K. M. Newaz · Kirk D. Wallace · Samuel A. Wickline · Stuart A. Solin · Rashid Bashir

Published online: 11 June 2010

Abstract We report the electric field and pH sensitivity of fluid gated metal-semiconductor hybrid (MSH) Schottky structures consisting of a Titanium layer on n-type GaAs. Compared to standard field-effect sensors, the MSH Schottky structures are 21 times more sensitive to electric field of −46.6 V/cm and show about six times larger resistance change as pH of the solution is decreased from 8.17 to 5.54. The potential change at the fluidic gate and passivation layer interface by bias voltages and pH are mirrored by the metal shunt, resulting in larger depletion widths under the Schottky junction and resistance change as compared to sensors with no Schottky junction. 2D numerical simulation results are in good agreement with the measured data and suggest thinner mesa with lower doping density can further increase device sensitivity.

Keywords Field effect biosensor · Schottky junction · Fluidic measurement · Electric field sensing

W.-J. Chang · H.-J. Suk · R. Bashir (✉)
Department of Electrical and Computer Engineering, Department of Bioengineering, Micro and Nanotechnology Laboratory, University of Illinois at Urbana-Champaign, Urbana, IL 61801, USA
e-mail: rbashir@illinois.edu

A. K. M. Newaz · K. D. Wallace · S. A. Wickline · S. A. Solin (✉)
Department of Physics and Center for Materials Innovation, Washington University in St. Louis, Brookings Drive, St. Louis, MO 63130, USA
e-mail: solin@wuphys.wustl.edu

S. A. Solin
Blackett Laboratory, Imperial College London, Prince Consort Rd., London SW7 2BZ, UK

Present Address:
A. K. M. Newaz
Department of Physics and Astronomy, Vanderbilt University, 6301 Stevenson Center, VU Station B #351807, Nashville, TN 37235, USA

1 Introduction

Semiconductor-based devices have been actively studied as chemical and biological sensors due to label-free detection, ease of miniaturization, low-cost fabrication, and simple integration into microelectronic circuits (Park et al. 2005). For example, ion-sensitive field-effect transistors (ISFET) have been used for the detection of pH (Bergveld 2003), DNA (Kim et al. 2008), and enzymes (Koch et al. 1999). Silicon nanowires as nanoscale diameter manifestations of ion-sensitive or chemical field effect transistors have been demonstrated as highly sensitive detectors for proteins (Cui et al. 2001) and DNA molecules (Hahm and Lieber 2004). DNA hybridization and charged peptide-RNA interactions were detected using polycrystalline silicon-based thin-film transistors (Estrela and Migliorato 2007) and gallium arsenide-based junction-field-effect transistors (Lee et al. 2008), respectively. To improve the sensitivity of these types of sensors, physical properties, such as carrier concentration and dopant type (Cui et al. 2000; Cui and Lieber 2001; Duan et al. 2001), as well as geometric properties, such as device shape and the dimensions (Popovic 1991; Elibol et al. 2008), have been modified.

An extraordinary electroconductance (EEC), a novel idea that utilizes the effect of both the physical properties of a Schottky interface and conduction through the metal contact in a metal-semiconductor-hybrid (MSH) structure, has been applied to the electric field sensing in non-

aqueous conditions (Newaz et al. 2009). However, electric field sensitivity of the MSH structures in aqueous conditions has not yet been examined. In this study, we report on the electric field sensing by the EEC MSH structures with a fluidic gate, and on the sensitivity amplification by geometric modifications. The effect of physical and geometrical adjustments on device sensitivity was also investigated using numerical simulations. Furthermore, chemical sensitivity of the MSH structures was tested using various pH solutions.

2 Material and methods

2.1 Device fabrication

A 650 μm thick (100) semi-insulating GaAs substrate (resistivity ~ 1.0–6.0×10^8Ω cm) with a 100 nm thick Si-doped n-GaAs epitaxial layer (N_d=4×$10^{17}$$cm^{-3}$) was used to fabricate the MSH structures. This three-layer substrate purchased from IQE Inc. contains the undoped GaAs layer to serve as the buffer layer that prevents the current leakage from the active layer to the semi-insulating substrate. The fabrication procedures are as follows. After depositing Cr/Au/NiCr alignment marks using photolithography and lift-off techniques, the active layer was patterned into a circular mesa with 7.8 μm diameter using the electron beam lithography (JBX-6000FS/E, Hitachi, Japan) and inductively coupled plasma reactive ion etch (ICP-RIE, SLR-770, PlasmaTherm, U.S.A.).

Figure 1(a), (b), and (c) show SEM images (S-4800, Hitachi, Japan) of three different types of sensors. The bare sensor shown in Fig. 1(a) does not have a shunt metal while the MSH structures shown in Fig. 1(b) and (c) contain a 2.5 μm×2.5 μm Ti/Au (40 nm/40 nm) shunt layer in the center of the mesa. Thus, a bare sensor shown in Fig. 1(a) required only one more electron beam lithography step to define AuGe/Ni/Au ohmic leads on the periphery of the mesa while the MSH structures shown in Fig. 1(b) and (c) needed the third electron beam lithography step for patterning shunt layer in the center of the mesa. The AuGe/Ni/Au contacts on the periphery of the mesa were annealed at 450°C for 2 min to make the contacts ohmic. Then an unannealed Titanium layer was deposited to form the Schottky junction at the Ti/n-GaAs interface. The sensor design depicted in Fig. 1(c), with the shunt layer connected to a contact pad, was used to study the properties of the Schottky junction via direct biasing. Each sensor was passivated with a silicon nitride (Si_3N_4) or an aluminum oxide (Al_2O_3) layer by plasma enhanced chemical vapor deposition (Mixed frequency PECVD, Surface Technology Systems PLC., U.K.) or thick atomic layer deposition (ALD), respectively, to prevent leakage between the fluidic gate and the mesa during measurements. The final thickness of silicon nitride was either a 20 nm or 50 nm for the characterization of the effect of thickness of the passivation layer on the measurement sensitivity. The thickness of aluminum oxide was 15 nm. Figure 1(d) shows the schematic side view of the sensor which has shunt metal layers with the fluidic gate.

2.2 Measurement

To characterize the Schottky interface of the MSH structure at room temperature, DC voltages from −1.5 V to 0.5 V were applied using E3612A DC power supply (Agilent, U.

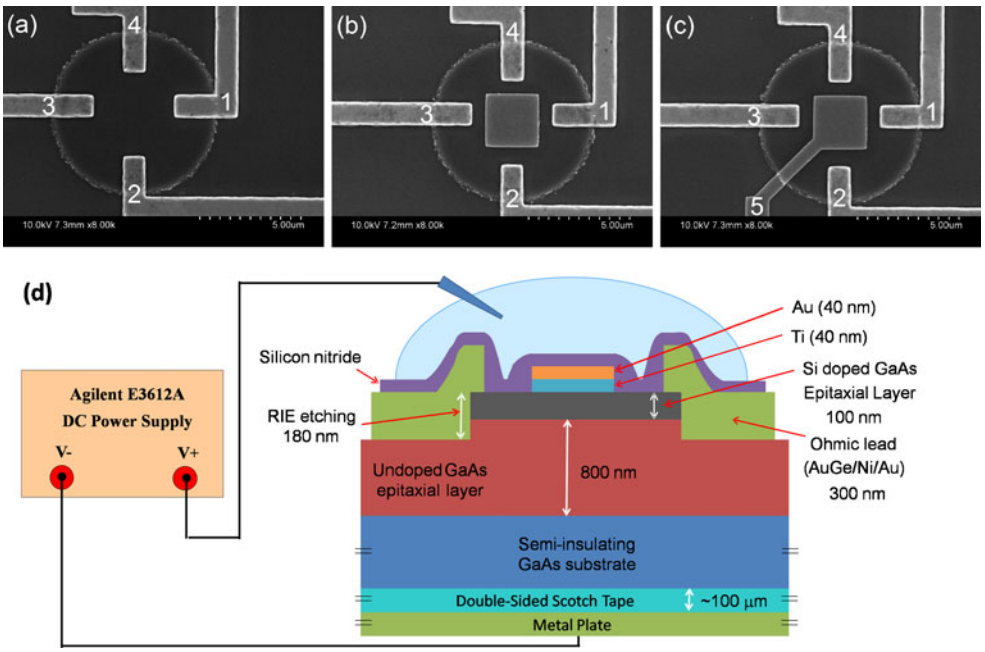

Fig. 1 (**a**) SEM images of 7.8 micron sensors without shunt metal, (**b**) with the isolated shunt metal, (**c**) with the shunt metal connected to contact pad via lead 5, (**d**) Schematic side view, dimensions of the sensor, and the set up for fluidic measurements. The DC power supply is used to generate an external electric field perpendicular to the sensor

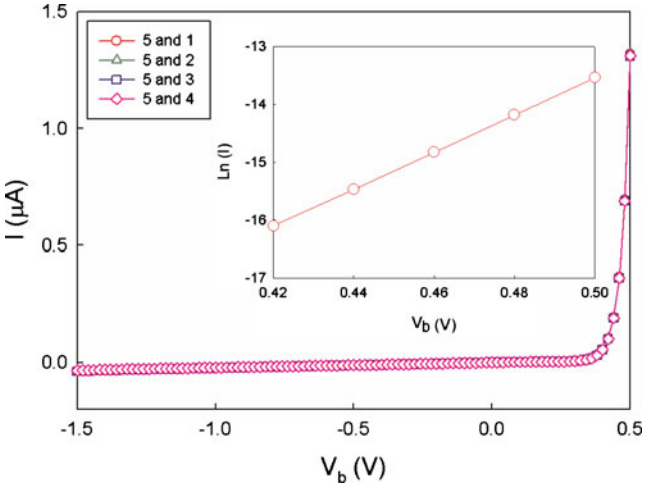

Fig. 2 Room temperature I-V characteristics of the Schottky interface with DC bias voltages across leads 5 and 1, 2, 3, or 4. Inset: natural log of I vs bias voltage for shunt voltages exceeding 0.42 V

S.A.) from lead 5 to lead 1, 2, 3 or 4 (Fig. 1(c)) while measuring the current through the selected pair of leads using HP 4155B (Agilent, U.S.A.) semiconductor parameter analyzer. Using four equally spaced ohmic leads on the periphery of the device, the 4-point-probe lock-in method was employed to eliminate contact resistance between the ohmic leads and the mesa while excluding the low frequency thermal noises. One KHz sinusoidal voltage from a function generator (33120A, Agilent, U.S.A.) was applied across a 20 MΩ resistor to produce a 200 nA current that was passed through leads 1 and 4. The voltage due to the current flow in the MSH structure was measured across leads 2 and 3 with a lock-in amplifier (SR850, Stanford Research Systems, U.S.A.), which was then divided by the injected current to calculate the effective sheet resistance.

The fluidic gate on top of the passivation layer was formed by flowing 10 mM phosphate buffered saline (PBS) (ATCC, U.S.A.) solution in a poly(dimethyl siloxane) (PDMS) (Sylgard 184, Dow Corning, U.S.A.) reservoir located on top of the sensor for 5 min. As shown in Fig. 1(d), the chip was adhered to the Au metal plate by a double-sided scotch tape (resistance ~10^{12}Ω) and a DC voltage was applied between the fluidic gate and the bottom metal plate to produce the electric field perpendicular to the MSH device. The electric field is a linear function of the fluidic gate voltage and can be expressed as

$$E(V_{fg}) = \frac{V_{fg}}{t_{total}}, \quad (1)$$

where V_{fg} and t_{total} are fluidic gate voltage and distance from the top of the passivation layer to the bottom of the double-sided scotch tape. For the fluidic gate voltages from − 3.5 V to +3.5 V, the electric fields produced were calculated to be from −46.6 V/cm to +46.6 V/cm, and the changes in the effective sheet resistance were measured to determine the electric field sensitivity of the MSH structure. For pH measurements, the pH value of the fluidic gate was altered by adding 1M of HCl or NaOH solution to the PBS solution.

3 Results and discussion

3.1 Characterization of Schottky junction

As shown in the main panel of Fig. 2, Schottky I-V measurements using different leads produced almost identical results due to the symmetry of the structure. Since the current transport across the Schottky interface with donor density ranging from 5×10^{16} to 5×10^{17} cm^{-3} is dominated

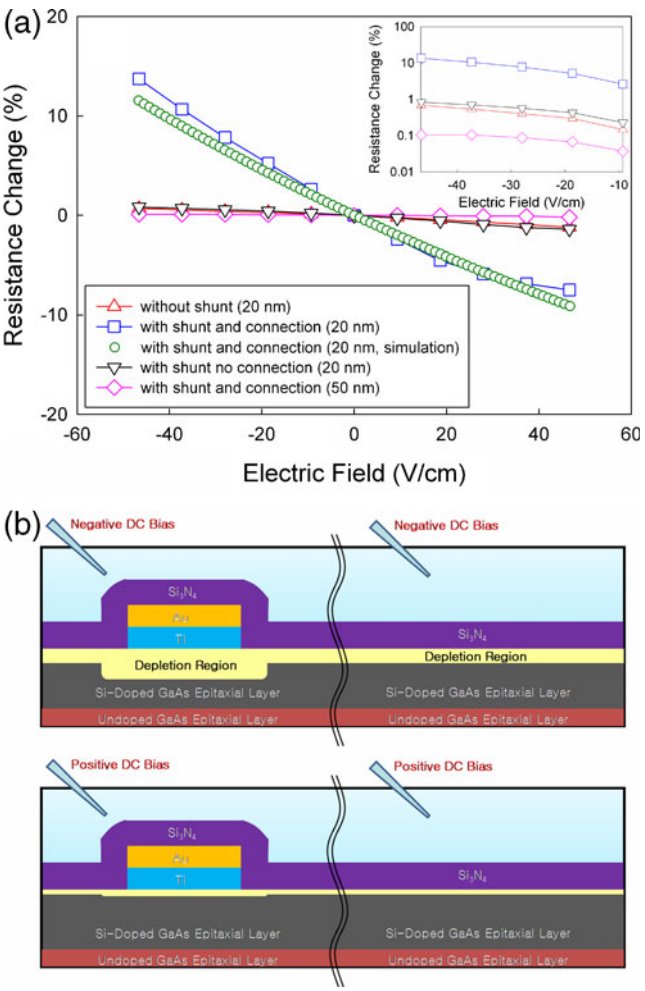

Fig. 3 (**a**) Effect of Si_3N_4 layer thickness and the shunt on the electric field sensitivity. Inset: Percent change in resistance on a log scale for negative electric field values. (**b**) Schematic side view of the sensing mechanism for negative and positive electric fields

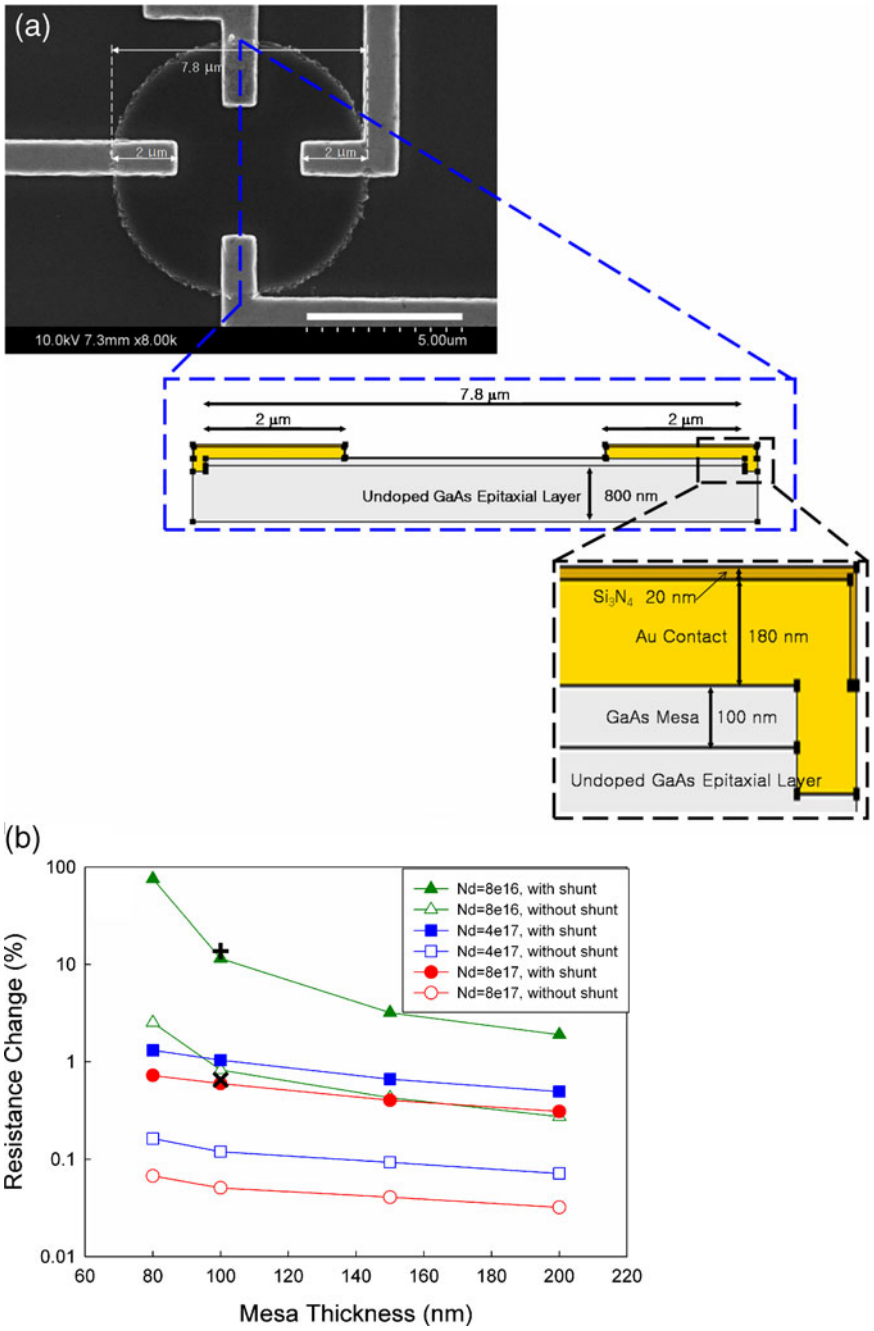

Fig. 4 (**a**) Schematic side view and dimension of the sensor used for the simulation by DESSIS. (**b**) Simulation results of the percent change in resistance at −46.6 V/cm for various combinations of the mesa thickness and the doping density. The experimental results at −46.6 V/cm for the sensors with (+) and without the shunt (×) are also shown

by thermionic field emission (Dushman 1930), the current density through our structure can be expressed as

$$I(V_b) = I_s[\exp(qV_b/nkT) - 1], \quad (2)$$

where V_b is the shunt voltage, I_s is the saturation current, and n is the non-ideality factor that usually varies between 1 and 2 (Duan et al. 2001).[11] If $n \approx 1$ and $V_b >> kT/q$, the equation becomes a simple exponential function, and $\ln(I(V_b))$ vs V_b plot as shown in the inset of Fig. 2 can be used to determine n and the Schottky barrier height, Φ_{bi}. n and Φ_{bi} at room temperature were found to be 1.2 eV and 0.690 eV, respectively.

3.2 Electric field sensitivity with a fluidic gate

Figure 3(a) shows the percent change of mesa resistance in response to the external electric field in fluid. As shown in the inset of Fig. 3(a), the change in resistance at −46.6 V/cm for the sensor with the shunt metal connected to a contact pad was increased by about two orders of magnitude (~192 times), after thinning the Si_3N_4 layer from 50 nm to 20 nm. For the 20 nm thick passivation, the structure with the shunt metal (Fig. 1(b)) showed only a slight improvement in sensitivity compared to the sensor without the shunt. The resistance of both sensors increased

monotonically as electric field was decreased from +46.6 to −46.6 V/cm, and the sensor with the shunt showed only 0.14% and 0.20% increase in percent change at −46.6 and +46.6 V/cm respectively. Interestingly, the sensor with the shunt metal connected to a contact pad exhibited much higher sensitivity, with 21 times larger percent change at −46.6 V/cm than the sensor without the shunt.

The enhanced sensitivity of the sensor with the shunt connected to the contact pad is due to efficient mirroring of the fluidic gate voltage, V_{fg}, by the shunt metal. The voltage at the shunt, V_{shunt}, which modulates the depletion width at the Ti/n-GaAs interface, is a function of V_{fg} and can be expressed as

$$V_{shunt} = V_{fg} \cdot C_{control} / \left(C_{parasitic} + C_{control}\right), \quad (3)$$

where $C_{control}$ and $C_{parasitic}$ are capacitances between the fluidic gate and the shunt and between the shunt and the GaAs mesa, respectively. Since $C_{control}$ for the sensor with the isolated shunt is comparable in magnitude to $C_{parasitic}$, V_{shunt} is only a fraction of V_{fg}. On the other hand, the sensor with the shunt metal connected to a contact pad has a much larger $C_{control}$, because $C_{control}$ is a linear function of the overlap area between the fluidic gate and the shunt. As a result, $C_{control} / \left(C_{parasitic} + C_{control}\right) \approx 1$ and $V_{shunt} \approx V_{fg}$ for the sensor with the shunt connected to the contact pad. For the same V_{fg}, the depletion region under the shunt and the resistance of the GaAs mesa are thus modulated much more significantly by the sensor with the shunt connected to the contact pad.

The sensors with the shunt metal connected to a contact pad show lower sensitivity for positive electric fields, with only 6.1 times larger percent change at +46.6 V/cm compared to the sensor without the shunt. This asymmetrical effect of the shunt on the electric field sensitivity is due to the change in the depletion region thickness as a function of the external electric field. Negative fluidic gate voltages make the depletion region thicker at both the Ti/n-GaAs interface (underneath the shunt) and at the Si_3N_4/n-GaAs interface (mesa region not covered by the shunt). However, the area covered by the shunt is depleted much more than the uncovered areas due to the presence of the Schottky built-in potential, which creates a depletion region even in the absence of any external perturbation. As shown in Fig. 3(b), when a positive electric field is applied to the sensors, the depletion region shrinks until the difference between the area covered by the shunt and the uncovered area becomes negligible. Since the GaAs mesa resistance is directly related to the depletion region thickness, the Schottky junction between the shunt and the n-GaAs mesa amplifies the change in resistance more significantly for negative electric fields than for positive. Moreover, the resistance of the sensor with the shunt starts to level off as the external electric field strength exceeds 18.6 V/cm. The GaAs mesa resistance, R_{GaAs}, which is related to the reciprocal of the thickness of the undepleted region, $t_{undepleted}$, can be expressed as

$$R_{GaAs} = \beta / t_{undepleted} = \beta / (t - W(E)), \quad (4)$$

where β is a constant, t is the mesa thickness, and $W(E)$ is the depletion region thickness as a function of external electric field, E. The slope of the change in resistance, dR_{GaAs}/dE, is thus a function of $t_{undepleted}^{-2}$ and dW/dE. For a small range of electric field strengths, dW/dE is relatively constant while $t_{undepleted}$ becomes larger as the electric field becomes more positive, which results in small dR_{GaAs}/dE and a saturated R_{GaAs}.

3.3 Numerical simulations

Using the 2D numerical device simulator (DESSIS, Integrated Systems Engineering, Inc., U.S.A.), the measured percent change in resistance for the sensor with the shunt passivated with a 20 nm thick Si_3N_4 layer was compared to the simulation result. After simplifying our structure into a 2D model as shown in Fig. 4(a), the percent changes in resistance due to the external electric field ranging from −46.6 to +46.6 V/cm were simulated with the Schottky barrier height of 0.69 eV (from the inset of Fig. 2), $N_d = 8 \times 10^{16} cm^{-3}$ (from the 4-point probe resistance measurements of sensors without the shunt), and a Si_3N_4/n-GaAs interface trap state density

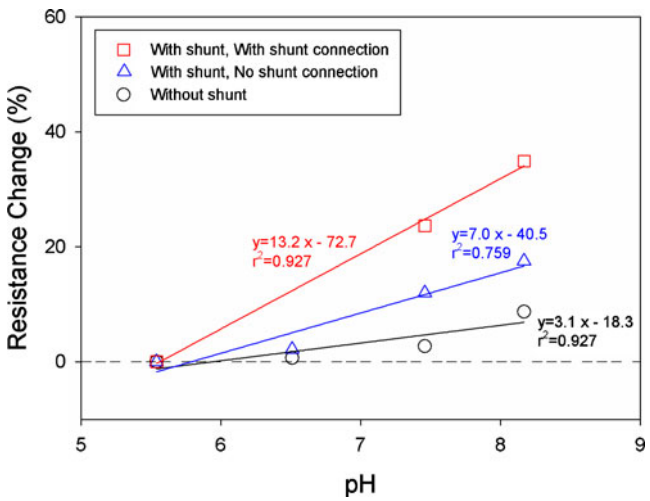

Fig. 5 Resistance change of three different types of sensors in response to the changes in pH of the fluidic gate when the fluidic gate bias was decreased from 0 V to −2.5 V. The percent change in resistance of each sensor type was normalized based on their measured result at pH5.54

of $1\times10^{14}eV^{-1}cm^{-2}$(Wieder 1983). As shown in Fig. 4(b), the numerical simulation results were very close to the actual data, with the maximum difference of 2.2% in percent change at −46.6 V/cm. To determine the effect of physical parameters on the sensor sensitivity, various combinations of the n-GaAs mesa thickness and doping density were also analyzed using DESSIS. As shown in Fig. 4(b), higher sensitivity was obtained with lower doping density for all the mesa thicknesses for both the sensor with and without the shunt. For instance, when the mesa thickness was kept at 100 nm while the doping density was reduced from $8\times10^{17}cm^{-3}$ to $8\times10^{16}cm^{-3}$, the sensitivity increased by a factor of 19.3 and 16.2 for sensors with and without the shunt, respectively, at −46.6 V/cm. A thinner mesa amplified the response of both sensors when the doping density was fixed, but the sensor with the shunt showed much higher improvement in sensitivity at lower doping densities. At $N_d=8\times10^{17}$ cm^{-3}, the sensor response at −46.6 V/cm was increased by a factor of 2.3 and 2.1 for the sensors with and without the shunt, respectively, as the mesa thickness was reduced from 200 nm to 80 nm. However, for a lower N_d (8×10^{16} cm^{-3}), the resistance of the sensor with the shunt was increased by a factor of 39.8, which was over four times higher than a factor of 9.3 improvement shown by the sensor without the shunt as the mesa thickness changed from 200 nm to 80 nm.

3.4 pH sensitivity

The resistance change of the sensors for each pH was determined by calculating the percent increase in resistance at the fluidic gate bias of −2.5 V compared to that at 0 V. Figure 5 shows the resistance change normalized by the result from pH5.66 for each type of structure. At pH8.17, the normalized resistance change of the sensor with the shunt metal connected to a contact pad was 1.35, which is over 80% higher than the change observed from the sensor without the shunt. These four terminal device topologies have the advantage of offering a four point resistance measurement, hence eliminating any issues due to variations in contact resistance. However, the devices with the shunt metal have a parasitic current path around the shunt metal, which could result in a smaller change in response compared to two terminal device layouts. This could also explain the fact that the observed changes in response due to pH were limited to 20–40%. It should be noted that the larger resistance change of the sensor with the shunt layer connected to a contact pad is consistent with the earlier measurement and are due to the efficient mirroring of surface potential and larger changes depletion widths explained earlier in the text.

4 Conclusion

Our results demonstrate that the presence of a Schottky interface between the shunt and the GaAs mesa significantly improves the sensitivity as demonstrated in wet conditions, especially for negative electric fields. Thinner nitride layer also increase the sensor response to the external electric field as expected. Moreover, the simulation results suggest that thinning the mesa and lowering the doping density of the GaAs epilayer would improve the sensitivity, especially for the sensor with the shunt. pH sensing by MSH structures also proves that the sensitivity amplification by the Schottky interface is not limited to electric fields, but can be applied to biological and chemical sensing. After further optimization of device dimensions and physical parameters, the MSH structure could be used as a highly sensitive electric field and charge sensor in fluidic environments. For example, a change in surface charge density on the functionalized passivation layer due to pH, biological or chemical molecules can be measured to monitor DNA hybridization, enzyme reaction, and antibody-antigen interaction, etc.

Acknowledgements This work was supported by the U.S. NIH under Grant 1U54CA11934201. S.A.S. also received support from the U.S. NSF under Grant ECCS-0725538. S. A. S., S. A. W., and K. D. W. are cofounders of and have a financial interest in PixelEXX, Inc. a start-up company whose mission is to market imaging arrays. W.J.C. was partially supported from the ERC for Advanced Bioseparation Technology, KOSEF, Korea. Two of the authors (W.J.C. and H.J.S.) contributed equally to this work.

References

A.K.M. Newaz, Y. Wang, J. Wu, S.A. Solin, V.R. Kavasseri, I.S. Ahmad, I. Adesida, Phys. Rev. B **79**, 195308 (2009)
C.-H. Kim, C. Jung, H.G. Park, Y.-K. Choi, Biochip J. **2**, 127–134 (2008)
H.H. Wieder, Surface Science **132**, 390–405 (1983)
J.W. Park, H.S. Jung, H.Y. Lee, T. Kawai, Biotechnol. Bioproc. Eng. **10**, 505–509 (2005)
J.-I. Hahm, C.M. Lieber, Nano Lett. **4**, 51–54 (2004)
K. Lee, P.R. Nair, M.A. Alam, D.B. Janes, H.P. Wampler, D.Y. Zemlyanov, A. Ivanisevic, J. Appl. Phys. **103**, 114510 (2008)
O.H. Elibol, B. Reddy Jr., R. Bashir, Appl. Phys. Lett. **92**, 193904 (2008)
P. Bergveld, Sens. Actuators B **88**, 1–20 (2003)
P. Estrela, P. Migliorato, J. Mater. Chem. **17**, 219–224 (2007)
R.S. Popovic, *Hall effect devices* (dam Hilger, Bristol, 1991)
S. Dushman, Rev. Mod. Phys. **2**, 381–476 (1930)
S. Koch, P. Woias, L.K. Meixner, S. Drost, H. Wolf, Biosens. Bioelectron. **14**, 413–421 (1999)
X. Duan, Y. Huang, Y. Cui, J. Wang, C.M. Lieber, Nature **409**, 66–69 (2001)
Y. Cui, C.M. Lieber, Science **291**, 851–853 (2001)
Y. Cui, Q. Wei, H. Park, C.M. Lieber, Science **293**, 1289–1292 (2001)
Y. Cui, X. Duan, J. Hu, C.M. Lieber, J. Phys. Chem. B **104**, 52135216 (2000)